

RoboDuet: A Framework Affording Mobile-Manipulation and Cross-Embodiment

Guoping Pan^{*1}, Qingwei Ben^{*1,3}, Zhecheng Yuan^{1,2,3}, Guangqi Jiang^{2,4},
Yandong Ji⁵, Jiangmiao Pang³, Houde Liu¹, Huazhe Xu^{1,2,3}

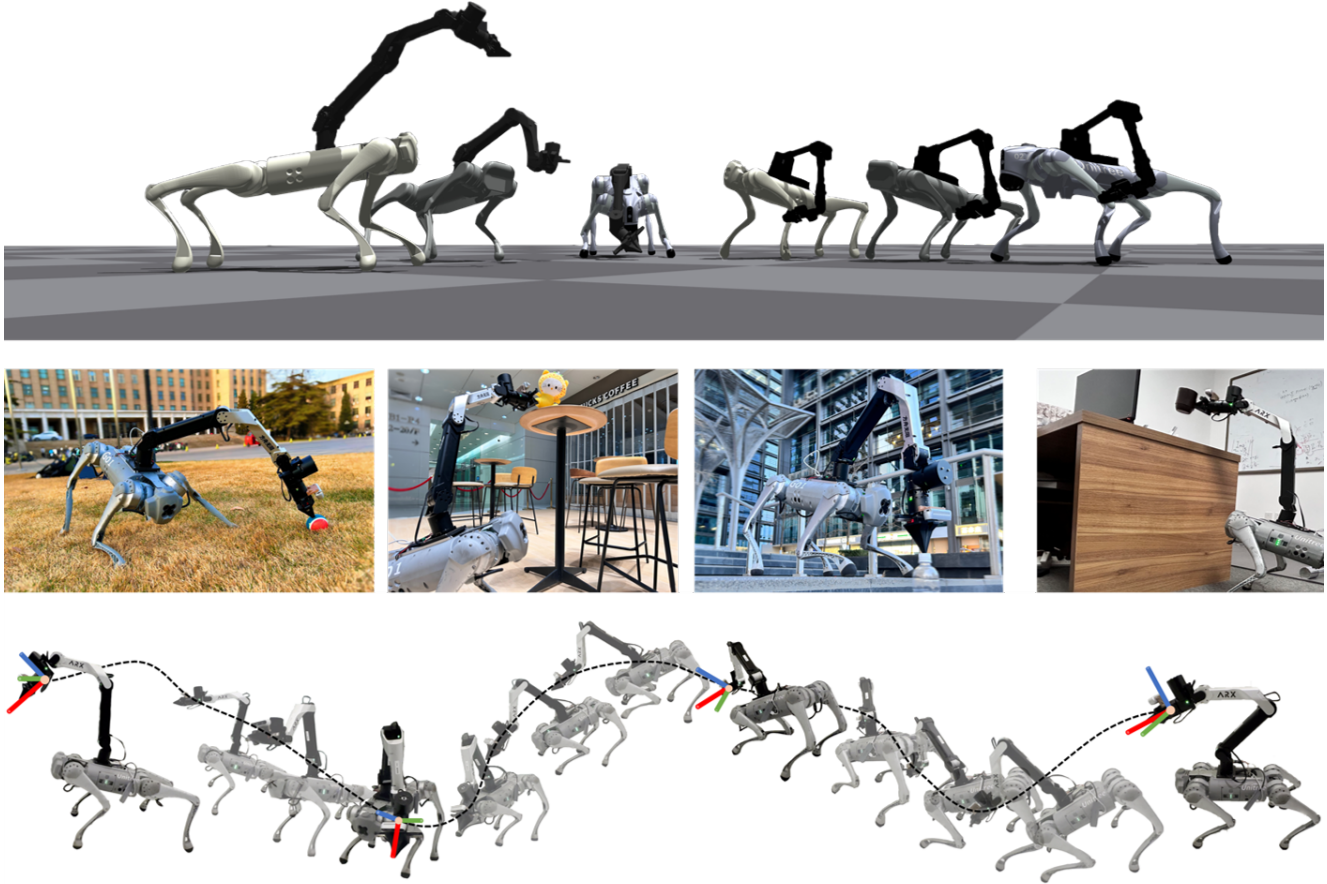


Fig. 1: RoboDuet affords mobile-manipulation and cross-embodiment **Top row:** Training combinations of two arms and three dogs in simulation with RoboDuet, we achieve effective policies for all six settings. After replacing some components, it's not necessary to retrain policies for the unchanged one, demonstrating the capability for cross-embodiment. **Middle row:** From left to right, the robot walks to picks up a small ball on grass, grasps a doll from a high table in a café, grabs a bottle on lower stairs, and picks up a cup on an office desk. These tasks fully demonstrate our policy's capability of mobile manipulation. **Bottom row:** We give the robot several commands, and it follows them precisely in real world and maintains stability across various body pose transitions.

Abstract—Combining the mobility of legged robots with the manipulation skills of arms has the potential to significantly expand the operational range and enhance the capabilities of robotic systems in performing various mobile manipulation tasks. Existing approaches are confined to imprecise six degrees of freedom (DoF) manipulation and possess a limited arm workspace. In this paper, we propose a novel framework,

RoboDuet, which employs two collaborative policies to realize locomotion and manipulation simultaneously, achieving whole-body control through interactions between each other. Surprisingly, going beyond the large-range pose tracking, we find that the two-policy framework may enable cross-embodiment deployment such as using different quadrupedal robots or other arms. Our experiments demonstrate that the policies trained through RoboDuet can accomplish stable gaits, agile 6D end-effector pose tracking, and zero-shot exchange of legged robots, and can be deployed in the real world to perform various mobile manipulation tasks. Our project page with demo videos is at <https://locomanip-duet.github.io>.

^{*}Authors with equal contribution. ¹Tsinghua University ²Shanghai Qi Zhi Institute ³Shanghai AI Lab ⁴Sichuan University ⁵UC San Diego. Correspondence to: Guoping Pan <pgp23@mails.tsinghua.edu.cn>, Qingwei Ben <bqw20@mails.tsinghua.edu.cn>, Huazhe Xu <huazhe_xu@mail.tsinghua.edu.cn>.

I. INTRODUCTION

In recent years, mobile robots have increasingly been deployed to assist humans and demonstrated remarkable capabilities [1]–[5]. Typically, these robots operate on wheeled or tracked bases, equipped with arms that have a limited workspace. This limitation has sparked interest in developing legged robots to undertake manipulation tasks, offering enhanced versatility and adaptability in diverse environments. By employing whole-body control in legged robots and arms, it is possible to effectively overcome terrain constraints and significantly expand the manipulation workspace of the arm [6]–[10]. However, training a legged loco-manipulation robot to achieve whole-body control like humans, along with accurate pose tracking capabilities, presents a substantial challenge to researchers.

As a pioneering effort in this domain, Fu et al. [8] has utilized a unified control policy to accomplish coordinated manipulation and locomotion. This approach leverages advantage mixing to facilitate the simultaneous control of both the arms and legs, and regularized RMA [11] for further narrowing the sim-to-real gap. Despite the implementation of a whole-body control framework, it cannot tackle accurate 6D pose tracking within the workspace, a capability that is crucial for manipulation tasks. On the other hand, while GAMMA [9] and GeFF [10] are capable of grasping objects based on 6-DoF end-effector control, their operation strategies separate the arm and the quadruped mechanisms, thus falling short of achieving whole-body control. This distinction restricts the arm’s working space. Hence, achieving wide-range manipulation tasks throughout the entire space requires a novel training paradigm, which not only necessitates more consistent coordination between the quadruped and the arm but also improves the training efficiency and generalization ability.

In awareness of these challenges, we introduce the **RoboDuet**: an integrated legged loco-manipulation framework tailored for large-range 6D pose tracking. The training process for RoboDuet is structured in two stages. In stage 1, we refine a locomotion policy to endow the legged robot with essential mobility capabilities. On top of stage 1, stage 2 involves training an arm policy that may coordinate with the locomotion policy. We argue that employing a two-phase training strategy enhances the stability of the training process, resulting in the acquisition of highly precise and large-range 6-DoF tracking agents.

The interaction between the locomotion policy and the arm’s actions exhibits a duet performance, where the locomotion policy utilizes the actions of the arm as guidance to adjust its posture, while the arm complements the actions of the locomotion policy aiming to expand the robot’s workspace. This paradigm enables the arm to generate a 6D pose, directing the legged robot to synchronize with the arm, and thoroughly achieving comprehensive spatial 6D pose tracking. Furthermore, since the locomotion policy can be fixed in stage 2, RoboDuet can endow the robot with

the ability of cross-embodiment deployment among different quadrupeds. If you have different trained quadrupeds in hand from stage 1, their locomotion policies can be directly zero-shot combined with the arm policy trained in stage 2 for *performing*, and accomplishing the tasks with the partner arm. This mechanism can greatly reduce the training cost and obtain a more generalizable policy that can be applied to different embodiments.

Our contributions are summarized as follows:

- We propose a framework that can simultaneously achieve robust locomotion and agile 6D end-effector pose tracking, thus capable of mobile manipulation.
- Our framework effectively coordinates the dog and the hand with two collaborative yet separated policies, introducing the ability of cross-embodiment deployment.
- We conduct extensive simulation and real-world experiments to demonstrate the tracking accuracy, gait stability, and cross-embodiment ability of our framework.

II. RELATED WORKS

A. Mobile Manipulation

To expand the operating space of robotic arms by eliminating the constraints of a fixed base, significant efforts have been taken to achieve mobile manipulation. This involves integrating a movable chassis with an upper robotic arm, aiming to enable the robotic system to perform tasks such as opening doors, organizing rooms, etc. [1]–[4], [12]–[14]. However, moveable chassis inherently lacks the ability to traverse complex terrains or climb stairs, which limits the robot’s ability to perform mobile manipulation in diverse environments.

B. Learning-based Locomotion

Learning-based algorithms, especially deep reinforcement learning (DRL), have significantly advanced the locomotion of quadruped robots [15]–[23]. In contrast to their control-based counterparts, which require extensive engineering for accurate physical modeling of dynamics [24], [25], learning-based algorithms rely primarily on straightforward reward functions to develop robust locomotion policies. Physics simulators represented by IsaacGym [26] enable efficient data sampling and the acquisition of privileged observations in simulations. Techniques such as RMA [27] and domain randomization have effectively reduced the sim2real gap. Currently, learning-based locomotion rivals its traditional model-based control counterparts in adaptability to navigate difficult terrains, climb stairs [11], [28]–[30], and perform parkour [31], [32].

C. Whole-body Control for Legged Robot

Given the superior locomotive capabilities of quadruped robots compared to chassis, there is an emerging interest in developing whole-body control for integrating legged robots and robotic arms to finish mobile manipulation tasks. The current technological landscape features three primary strategies. The first involves control-based techniques like

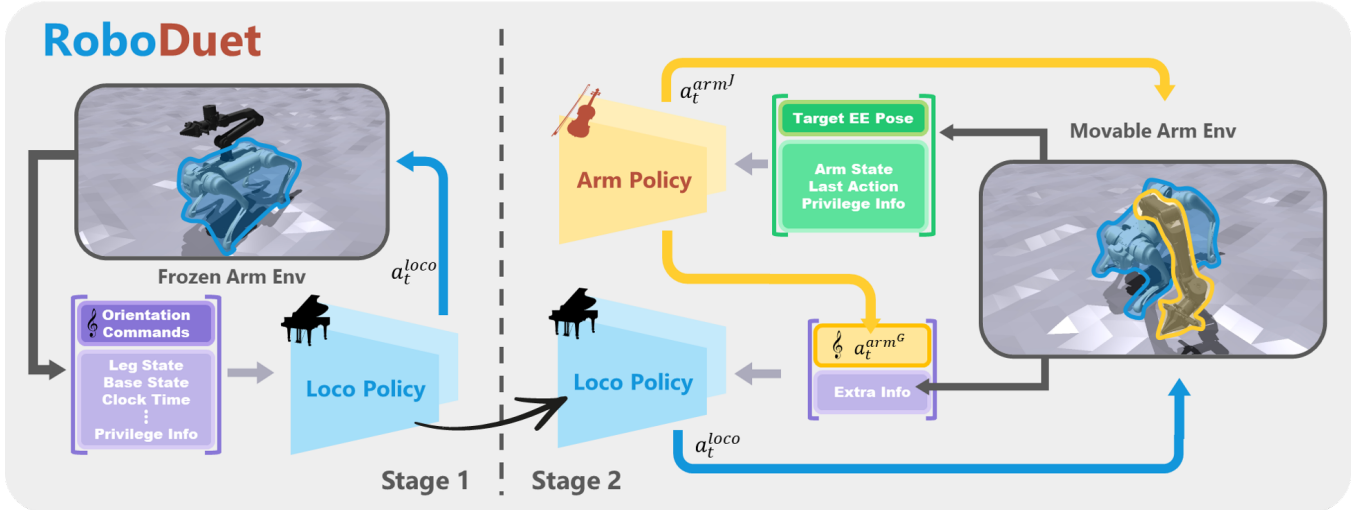


Fig. 2: RoboDuet consists of two stages. In Stage 1, the legged robot is trained to learn a loco policy with arm fixed. The loco policy inputs body orientation commands, proprioceptive states, and privileged information, and outputs action a_t^{loco} for each joint to achieve specific loco goals. In Stage 2, the loco policy and the arm policy are trained simultaneously. The loco policy from Stage 1 is used, taking the same inputs while the body orientation commands are provided by the arm policy. The arm policy is trained to achieve given 6D poses by taking the target end-effector pose and other observations as input and outputting actions $a_t^{arm^j}$ for each joint, as well as body orientation commands for the locomotion policy.

model predictive control (MPC), which require extensive engineering efforts and generally exhibit limited adaptability and robustness in complex environments [6]. The second strategy adopts learning algorithms to generate high-level velocity commands for legged robot, which are then translated into low-level joint control instructions based on motion APIs [7], [9], [10]. However, these approaches lack effective coordination between the legged platform and the arm, thus failing to maximize the potential for pitch and roll adjustments of legged robot to extend the operational range of the arm. The third approach leverages DRL to realize whole-body control. To date, applications in this domain have only achieved precise tracking of end-effector positions but have shown limited capability in either managing the end-effector’s orientation or navigating complex terrains [8]. Consequently, there is a clear need for innovative frameworks that are capable of harnessing the full locomotive advantages of quadruped robots while ensuring seamless coordination between the upper arm and the lower legged platform.

III. METHODS

A. Cooperative policy for whole-body control

RoboDuet consists of a **loco policy** for locomotion and an **arm policy** for manipulation. The two policies are harmonized as a whole-body controller. Specifically, the loco policy adjusts its actions accordingly by following instructions from the arm policy. For each policy, we implement reinforcement learning algorithms to maximize the discounted expected return $\mathbb{E}_{\pi_\theta} \left[\sum_{t=0}^{T-1} \gamma^t r_t \right]$ to find the optimal parameters θ , where r_t represents the reward at time step t , γ is the discount factor, and T is the maximum episode length. We utilize the Proximal Policy Optimization (PPO) algorithm for training.

Loco policy. The goal of the loco policy π_{loco} is to follow a target command $\mathbf{c}_t = (v_x^{cmd}, \omega_{yaw}^{cmd}, \phi_{pitch}^{cmd}, \phi_{roll}^{cmd})$. Since the center of mass offset caused by the additional manipulator will increase the risk of turnovers, we limit our velocity command to the linear velocity of the dog head pointing v_x^{cmd} and remove the lateral speed command. ω_{yaw}^{cmd} is the yaw angular velocity of the base. $\phi_t^{cmd} = (\phi_{pitch}^{cmd}, \phi_{roll}^{cmd})$ denotes the desired pitch and roll angle of the base. The observation of loco policy o_t^{loco} contains leg states $s_t^{leg} \in \mathbb{R}^{26}$ (leg joint positions and velocities), base states s_t^{base} (roll and pitch angles), target commands \mathbf{c}_t , clock time \mathbf{t}_t and last leg action $a_{t-1}^{leg} \in \mathbb{R}^{12}$. The leg action a_t^{leg} represents a target joint position offset that is added to the default joint position to specify the target position for twelve leg joint motors.

The reward of loco policy consists of three parts: $r_t^{loco} = r_t^{follow} + r_t^{gait} + r_t^{reg}$. The reward r_t^{follow} is designed to follow commands via locomotion. The reward r_t^{gait} promotes the execution of a robust gait, while the regularization component r_t^{reg} enhances the smoothness and safety of motion. As the aforementioned rewards are closely associated with stage 1, we will provide a detailed discussion of them in Section B.1.

Arm policy. The goal of the arm policy π_{arm} is to accurately track the 6D pose. The observations of arm policy o_t^{arm} is composed of arm states $s_t^{arm} \in \mathbb{R}^{12}$ (arm joint positions and velocities), target end-effector pose $\chi_t \in \mathbb{R}^6$, base states s_t^{base} , last arm action $a_{t-1}^{arm} \in \mathbb{R}^8$. The actions of the arm policy consist of two parts: the first six actions $a_t^{arm^j} \in \mathbb{R}^6$ represent the target joint position offsets corresponding to six arm joint actuators. Then, it will be concatenated with the output of the loco policy to achieve synchronous control of the overall system. It should be mentioned that the

position targets are tracked using a proportional-derivative controller. To expand the manipulation workspace with the whole body control, the rest part of the arm policy $a_t^{arm^G} = (a_t^{arm_p^G}, a_t^{arm_r^G}) \in \mathbb{R}^2$ is used to replace ϕ_t^{cmd} , providing additional degrees of freedom for end-effector tracking to cooperate with the loco-policy.

The reward of the arm policy contains two components: $r_t^{arm} = r_t^{manip} + r_t^{reg}$. Manipulation task reward r_t^{manip} is related to the end-effector tracking error, and the regularization component r_t^{reg} aims to improve the smoothness of manipulation. As shown in 3, building upon the trained loco policy, the arm policy will be activated in stage 2 for learning the large-range 6 DoF manipulation. We will provide a detailed discussion in Section B.2.

B. Two stage training

a) *Stage 1:* Stage 1 focuses on obtaining the robust locomotion capability. To ensure that the leg movements adapt to the center of mass and the inertia offset of the whole robot throughout the entire training process, we keep all the arm joints fixed at their default positions $(0, 0.8, 0.8, 0, 0, 0)$. In this stage, the arm policy is inactive, and the target end-effector pose p_t is set to zero. Inspired by the powerful blind locomotion algorithm [30], we apply a vector of behavior parameters b_t to represent a similar heuristic gait reward. Since our goal is to achieve pose tracking rather than diverse locomotion behaviors, we fix some gait parameters to speed up the convergence of training.

$$b_t = [\theta^{cmd}, f^{cmd}, h_z^{cmd}, \phi_{pitch}^{cmd}, \phi_{roll}^{cmd}, s^{cmd}, h_z^{f,cmd}] \quad (1)$$

where $\theta^{cmd} = (\theta_1^{cmd}, \theta_2^{cmd}, \theta_3^{cmd})$ are the timing offsets between pairs of feet. We choose to set it to $(0.5, 0, 0)$ for performing stable trotting gait. In order to enable the loco-policy to recognize the rhythm of stepping, the clock time $\mathbf{t}_t = [\sin(2\pi t^{FR}), \sin(2\pi t^{FL}), \sin(2\pi t^{RR}), \sin(2\pi t^{RL})]$ is computed from the offset timings of each foot: $[t^{FR}, t^{FL}, t^{RR}, t^{RL}] = [t + \theta_2^{cmd} + \theta_3^{cmd}, t + \theta_1^{cmd} + \theta_3^{cmd}, t + \theta_1^{cmd}, t + \theta_2^{cmd}]$, where t is a counter variable that advances from 0 to 1 during each gait cycle and FR, FL, RR, RL are the four feet respectively. When the base velocity is zero, the jitter caused by marching on the spot will reduce the precision of manipulation. In this situation, we set clock time \mathbf{t}_t to one to force all the feet to maintain a stationary position. $f^{cmd} = 3\text{Hz}$ is the stepping frequency, h_z^{cmd} is the body height command which we set to zero to keep the body height to be 0.3m. $s^{cmd} = (s_x^{cmd}, s_y^{cmd})$ is the foot clearance which is set to $(0.45, 0.3)$. $h_z^{f,cmd}$ is the footswing height command, which we set to 0.06m.

Four gait-related rewards are formulated based on the behavioral parameter: $r_t^{gait} = r_t^{c_f^{cmd}} + r_t^{c_v^{cmd}} + r_t^{s^{cmd}} + r_t^{h^{cmd}}$. The first two components stand for utilizing penalties on foot contact force and the speed to drive the foot into the swing and stance states respectively. The Raibert Heuristic reward $r_{s^{cmd}}$ is used to compute the desired foot position in the

ground plane. The last term is used to standardize the peak height of the feet during the swing phase.

$$\begin{aligned} r_t^{c_f^{cmd}} &= \sum_{\text{foot}} \left[1 - C_{\text{foot}}^{cmd}(\theta^{cmd}, t) \right] \exp \left\{ -|\mathbf{f}^{\text{foot}}|^2 / \sigma_{cf} \right\} \\ r_t^{c_v^{cmd}} &= \sum_{\text{foot}} \left[C_{\text{foot}}^{cmd}(\theta^{cmd}, t) \right] \exp \left\{ -|\mathbf{v}_{xy}^{\text{foot}}|^2 / \sigma_{cv} \right\} \\ r_t^{s^{cmd}} &= \left(\mathbf{p}_{x,y,\text{foot}}^f - \mathbf{p}_{x,y,\text{foot}}^{f,cmd}(s^{cmd}) \right)^2 \\ r_t^{h^{cmd}} &= \sum_{\text{foot}} \left(h_{z,\text{foot}}^f - h_{z,\text{foot}}^{f,cmd} \right)^2 C_{\text{foot}}^{cmd}(\theta^{cmd}, t) \end{aligned} \quad (2)$$

where $C_{\text{foot}}^{cmd}(\theta^{cmd}, t)$ is the desired contact state of each foot computed from timing offsets, \mathbf{f}^{foot} , are the contact force with the ground plane and $\mathbf{v}_{xy}^{\text{foot}}$ are the horizontal speed of each foot. $\mathbf{p}_{x,y,\text{foot}}^f$, $\mathbf{p}_{x,y,\text{foot}}^{f,cmd}$ represent the current and desired foot position on the ground respectively. The desired foot position consists of clearance and offset that is calculated from current target speed. $h_{z,\text{foot}}^f$ is the current footswing height. Only when it is in the swing phase, will it approach the footswing height command. The gait reward helps to attain well-performed leg posture despite the extra weight brought by the robotic arm, providing a strong prior of locomotion capability for stage 2.

b) *Stage 2:* Stage 2 aims to coordinate locomotion and manipulation to achieve whole-body large-range mobile manipulation. The arm policy will be activated simultaneously with all the robotic arm joints. We adopt 6D spatial target pose of end-effector as policy input. To eliminate the influence brought by body rotation [8], we similarly use a posture-independent spherical coordinate to define the target end-effector pose χ_t . The target position of end-effector is represented by radius l , latitude p , and longitude y . To improve the accuracy of end-effector orientation tracking, we use Euler angles in Z-X-Y order for sampling, which can intuitively exclude many illegal postures, and convert them to included angle along each axis of the coordinate. The mathematical form of sampling can be expressed as follows:

$$R = R_Z \cdot R_Y \cdot R_X = \begin{bmatrix} r_{11} & r_{12} & r_{13} \\ r_{21} & r_{22} & r_{23} \\ r_{31} & r_{12} & r_{33} \end{bmatrix} \quad (3)$$

$$[\alpha, \beta, \gamma] = \left[\tan^{-1}\left(\frac{r_{21}}{r_{11}}\right), \tan^{-1}\left(\frac{r_{32}}{r_{22}}\right), \tan^{-1}\left(\frac{r_{13}}{r_{33}}\right) \right] \quad (4)$$

Here, R is the composite rotation obtained by sequentially rotating around the z-axis, y-axis, and x-axis. γ, β, α represent the included angles with corresponding axes. To ensure the error of the end-effector in position and orientation is reduced simultaneously, manipulation task reward r_t^{manip} can be constructed in exponential form.

$$r_t^{manip} = e^{-w \cdot \Delta l p y} \cdot e^{-\Delta \alpha \beta \gamma} \quad (5)$$

$$\begin{aligned}\Delta lpy &= \Delta l + \Delta p + \Delta y \\ \Delta \alpha\beta\gamma &= \Delta \alpha + \Delta \beta + \Delta \gamma\end{aligned}\quad (6)$$

where weight coefficient w is used to balance the priority of the two components.

IV. EXPERIMENTS AND RESULTS

A. Robot System

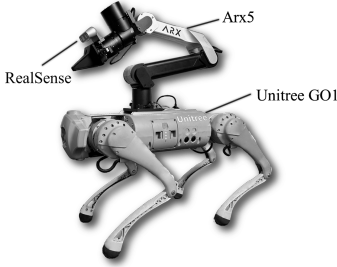


Fig. 3: Robot System

The robot system is composed of a 12-DoF legged robot Unitree Go1 Edu, and a robotic arm Arx5 which has 6 joints and a parallel gripper. Arx5's overall weight is 3.35kg, with a rated load capacity of 1.5kg. The robotic arm is mounted on the legged robot's back, and a RealSense D435i camera is mounted above the arm's gripper, ensuring that their relative poses remain unchanged. We deploy both the trained loco policy and the trained arm policy on the onboard computer Jetson Nano of Go1, and use AprilTag [33], [34] to get the target end-effector pose from the camera. Both power of Go1 and Arx5 are provided by Go1's onboard battery. Control frequency is 50Hz for both training and deployment.

B. Mobile Manipulation

TABLE I: Ranges of Commands used in training and evaluation

Parameter	Range	
	Trainig	Evaluation
v_x (m/s)	[-1.00, 1.00]	[-1.50, 1.50]
ω_z (rad/s)	[-0.60, 0.60]	[-1.00, 1.00]
l (m)	[0.30, 0.70]	[0.20, 0.80]
p (rad)	[-0.45, 0.45] π	[-0.50, 0.50] π
y (rad)	[-0.50, 0.50] π	[-0.50, 0.50] π
α (rad)	[-0.45, 0.45] π	[-0.50, 0.50] π
β (rad)	[-0.33, 0.33] π	[-0.50, 0.50] π
γ (rad)	[-0.42, 0.42] π	[-0.50, 0.50] π

1) *Experiment Setup*: To validate the significance of the two-stage training and the cooperative policy, which are key components of RoboDuet, we establish a **Baseline** algorithm training a unified policy in one-stage. The **Two-Stage** algorithm modifies this baseline by transitioning from one-stage to two-stage training, while the **Cooperated** algorithm builds on the baseline by replacing the unified policy with a cooperative policy. RoboDuet itself incorporates both two-stage training and cooperative policy. We train all algorithms for 45,000 iterations across 3 seeds, with the two-stage training comprising 10,000 iterations for stage 1 and 35,000 for stage 2, keeping the rest training components constant.

This process generates the corresponding policies for each algorithm.

To evaluate the performance of different policies, we assign random commands to the robots within the ranges shown in Table I. The goal is for the robots to achieve the target command within 4 seconds, and we then calculate the average error between the actual values and the target over the subsequent 2 seconds. We also measure the mean distance error D and mean angle error θ . To assess different policies' ability to maintain balance under external disturbance, we apply random forces ranging from 10 to 20 Newtons to the robots' bases and observe their survival rates. Additionally, to quantify manipulation capability more precisely, we consider a command completed when the tracking of the end-effector pose results in $D \leq 0.03\text{m}$ and $\theta \leq \pi/18$. We then calculate the workspace as the area of the convex hull formed by the points corresponding to these completed commands. We pick up five checkpoints spaced every 400 iterations backward from the maximum number of iterations, and the performance metrics are derived from an average of 60,000 simulations.

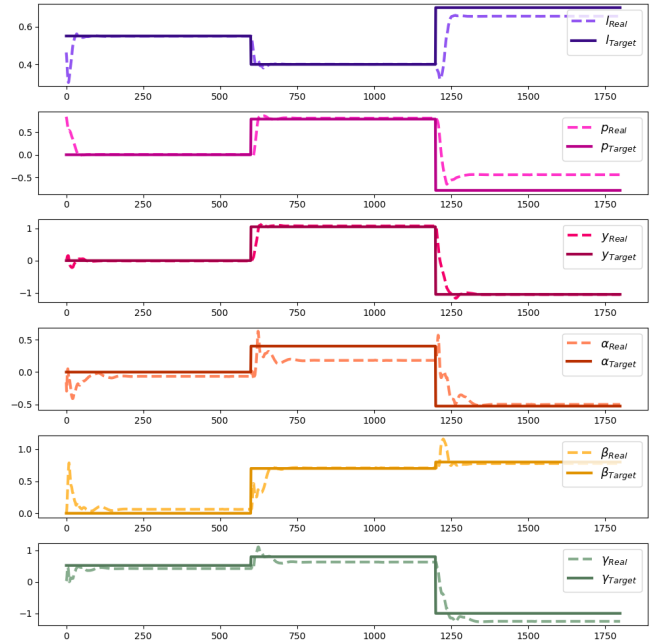


Fig. 4: Trajectory tracking curves of RoboDuet trained policy during periods of fixed commands and sudden changes.

2) *Results and Analysis*: Experiment results are listed in Table II, with best results for each metric highlighted in bold.

From the table, it is hard to say that Two-Stage performs better than Baseline on the given metrics. Both employ a unified policy, but with the same total number of training steps, Baseline dedicates more to whole-body control training. Conversely, Two-Stage allocates some training steps to locomotion gait training with all arm joints fixed, resulting in insufficient training for manipulation with whole-body control. Thus, Two-Stage is better in locomotion than Baseline, but lacks significant advantage in manipulation.

TABLE II: Metrics from various training methods (scaled by 10^{-2}). The initial three categories measure mean errors in robot velocity and end-effector position/orientation. The fourth assesses the robot’s survival rate against external forces, and the fifth evaluates the robot workspace. ”Still” tests occur with vel_x and ω_z at zero, while ”Move” tests are within command range limits.

Metrics		Still				Move			
		Baseline	Two-Stage	Cooperated	RoboDuet	Baseline	Two-Stage	Cooperated	RoboDuet
velocity tracking ↓	v_x (m/s)	0.95±0.34	0.81±0.19	0.66±0.03	0.49±0.07	12.49±2.48	10.39±0.35	12.13±0.99	10.16±1.05
	ω_z (rad/s)	0.83±0.50	0.42±0.12	0.47±0.03	0.35±0.05	52.12±0.45	52.97±0.38	51.29±0.22	51.53±0.67
position tracking ↓	l (m)	4.53±0.21	4.77±0.26	2.97±0.24	3.01±0.32	4.61±0.31	4.96±0.23	2.99±0.34	3.02±0.28
	p (rad)	22.96±1.99	20.75±2.99	17.87±1.12	17.65±2.05	21.12±0.46	19.60±3.49	18.15±0.91	17.66±2.01
	y (rad)	24.87±3.11	23.27±0.79	18.57±1.11	17.71±0.72	23.12±2.83	22.64±1.12	18.69±1.43	17.58±0.39
	D (m)	13.36±0.25	12.17±0.93	10.43±0.54	10.21±0.83	12.31±0.43	11.91±1.29	10.44±0.36	10.16±0.71
orientation tracking ↓	α (rad)	51.37±5.30	51.71±2.13	44.31±2.99	45.11±1.39	48.65±4.97	49.15±0.98	43.81±3.02	44.71±0.82
	β (rad)	90.68±10.24	89.91±8.83	79.48±3.56	75.80±2.65	90.83±10.26	88.92±6.45	78.09±3.05	75.70±2.53
	γ (rad)	83.94±11.32	78.43±3.36	66.21±1.87	64.78±2.25	82.88±10.07	76.98±4.50	66.43±1.71	65.24±2.22
	θ (rad)	92.50±4.85	93.69±3.99	82.32±1.86	84.08±3.13	92.39±5.64	94.62±4.33	81.99±1.39	83.88±3.23
survival rate (-) ↑		97.21±2.52	97.90±3.09	98.49±0.47	98.99±0.52	98.49±1.65	98.83±1.93	99.81±0.14	99.92±0.03
workspace (m^3) ↑		59.94±9.06	52.87±0.43	73.03±3.41	75.63±2.78	73.43±5.18	73.29±0.32	82.44±5.61	85.39±0.43

This indicates that unified policy and Two-Stage are incompatible, suggesting that simply adding two-stage training cannot enhance policy performance too much. In contrast, Cooperated and RoboDuet significantly surpass Baseline in all metrics. This indicates that within the same framework, a cooperative policy is more suitable for whole-body control in robots with multiple parts. Although Cooperated may perform slightly better in some metrics, RoboDuet excels in composite indicators D and θ , leading to a larger calculated workspace. Additionally, RoboDuet shows a higher survival rate under external forces than Cooperated, substantiating the positive impact of two-stage training on cooperative policy. Visualization in IsaacGym also reveals that without two-stage training, cooperative policy struggles to achieve true whole-body control, resulting in less natural gaits and less apparent coordination between the quadruped robot and arm, aligning with the metric outcomes. In summary, RoboDuet adeptly integrates cooperative policy and two-stage training, markedly enhancing control performance in tracking accuracy and gait stability, which proves that both ingredients are indispensable. Furthermore, we found that the robot’s workspace and survival rate are higher in a moving state, likely due to the robot’s ability to more effectively utilize its motion and arm coordination to counteract external forces, thereby offering enhanced robustness compared to a static state.

In Fig. 4, we present the variation in tracking error over time for a policy of RoboDuet, demonstrating its performance during periods of fixed commands and sudden changes. It can be observed that the policy converges quickly after the commands change, achieving stable velocity and end-effector pose. This indicates that the average error in the final third of the timesteps is reasonable and also demonstrates the stability and robustness of the policy we have trained.

C. Cross-Embodiment

1) *Experiment Setup:* To exhibit the cross-embodiment capability of RoboDuet, we select two additional quadruped robots (Unitree A1 and Unitree Go2). Both new embodiments robots possess 12 joints with three per leg. We place Arx5 on these legged robots and train the robot system with the same training method as stage 1. After convergence, we obtain specific loco policies for new embodiments. By directly combining the previously trained arm policy from Go1+Arx5 with the new loco policies, we test their workspaces and survival rates under external forces. Furthermore,

we expand the application of RoboDuet by incorporating WidowX 250s with each of the three legged robots, underscoring the system’s flexibility.

TABLE III: Workspace of Arx5 with different legged robots ($\times 10^{-2}$). RoboDuet achieves large-range workspace for different quadruped embodiments.

Arx+X	Workspace (m^3)	
	Still	Move
Go1	75.63±2.78	85.39±0.43
Go2	75.74±2.78	77.04±3.87
A1	74.51±3.22	80.32±2.82

This integration allows us to demonstrate that each combination can be efficiently trained using the same set of hyperparameters, minimizing the need for extensive adjustments. The effectiveness of these configurations is illustrated in the top row of Fig. 1, where they are depicted in various poses, showcasing the robust training outcomes across diverse robot embodiments.

2) *Results and Analysis:* As the results shown in Table III, even without additional training for the whole-body control capabilities of the new robot systems, the new combined robots can maintain excellent velocity tracking and pose tracking ability, which not only saves the training costs associated with introducing new equipment, but also greatly

demonstrate the superior zero-shot cross-embodiment capability of RoboDuet.

D. Real-World Deployment

In terms of real-world deployment, we craft three distinct types of tasks to validate the effectiveness of our policy in the real world and its proficiency in handling diverse mobile manipulation challenges. We deploy the RoboDuet policy in the real world on Go1+Arx5 and control the robot system in two different ways. The first involves utilizing camera to obtain the distance between the target end-effector pose and the current pose in real time, and the other employs the controller to pre-define the target end-effector pose relative to the base coordinate of the legged robot.

1) *End-effector Pose Tracking*: In this section, we use the first control method, where we manually manipulate the tag and use the camera placed at the end-effector to capture images. We apply the Apriltag algorithm to obtain the 6D pose of the tag marker in the camera coordinate system, which serves as the input for the trained policy. This input is used to obtain the real robot’s control information for manipulation. In practice, this manipulation method is equivalent to providing the robot with continuously changing commands in real-time. The experiment demonstrates that RoboDuet allows the robot to track the end-effector pose indicated by the tag in real-time. Additionally, when the robotic arm reaches the specified pose and the tag remains stationary, the attached arm can keep relatively stable at this position. This stability further indicates the effectiveness and robustness of RoboDuet in Sim-to-Real transfer.



Fig. 5: Pick up a plastic bottle with Apriltag.

2) *Trajectory Following*: While using the Apriltag method for control, the command is continuously changing, making it impossible to observe the performance of the real robot under sudden discrete command changes. Therefore, in this section, we employ the second method of variation, where we give the robot a fixed and unchanging command combination, maintain motion for a period of time, and then directly switch to another command combination. The robot will rapidly reach the posture required by the command after a brief adjustment while ensuring a relatively high stability.

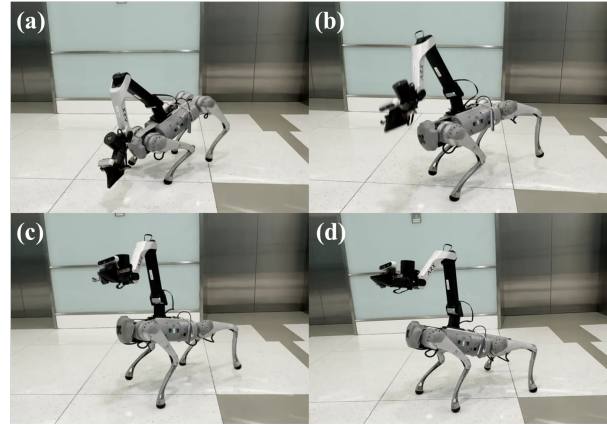


Fig. 6: A moment of the transition between two different discrete commands.

3) *Pick and Place*: Regarding the task of pick and place, we evaluate the robot’s ability to execute mobile manipulation tasks in various scenarios, including picking up a ball on a lawn, grasping a bottle downstairs, placing a cup on an office desk, grabbing a doll on a high table, all tasks are shown in Fig. 1 and are finished by both two kinds of control ways. In these tasks, the policy we trained is relatively stable and has a high success rate.



Fig. 7: Deployment of Baseline and RoboDuet in same environment and give same commands. **Left**: Failure case of Baseline. **Right**: Precise tracking of RoboDuet.

We attempted to deploy policies trained by the Baseline model in the real world, but, as illustrated in Fig. 7, these policies were unable to achieve the challenging poses that policies trained by RoboDuet could handle effortlessly in the same environment. Given the significant risks associated with further deployment, we decided against pursuing it further.

V. DISCUSSION AND LIMITATIONS

Our experiments demonstrate that the policy trained by RoboDuet outperforms the baseline, and verifies that both the cooperative policy and two-stage training solely are indispensable. On the opposite, our trained policy can precisely track velocity and 6D end-effector pose, adapt well to transitions between different command combinations, and show strong robustness against external disturbances. Additionally, RoboDuet enables cross-embodiment deployment, allowing hardware replacement without the need for retraining the

entire policy. The policy for unchanged components can be directly reused. The policy trained with RoboDuet can be directly deployed to real-world robots, exhibiting powerful tracking capabilities similar to those in simulations and completing various mobile manipulation tasks.

Due to the small field of view (FOV) of the RealSense D435i, it is challenging to get a complete view of the AprilTag when the end-effector approaches the target position. This makes using the AprilTag to obtain the target end-effector pose less robust. We have tried using AnyGrasp to infer the object pose, but its inference frequency is far below the desired 50Hz, and it cannot run onboard, making it unsuitable for the trained policy. Since this work mainly focuses on RL-based whole-body control, we have not further attempted to integrate vision-related content. In the future, we can try connecting state-of-the-art pose estimation algorithm and navigation module to achieve truly universal mobile manipulation.

VI. ACKNOWLEDGEMENT

We extend our gratitude to the ARX (Beijing) Technology Co., Ltd for providing us with their Arx5 arm, to Prof. Yang Gao and Ruiqian Nai from IIS, Tsinghua University for lending us a robotic dog, to Han Zhang and Huayue Liang for their hardware technical support, and to Shuzhen Li, Yi Cheng, and Gu Zhang for valuable discussions.

REFERENCES

- [1] P. Liu, Y. Orru, C. Paxton, N. M. M. Shafiullah, and L. Pinto, “Ok-robot: What really matters in integrating open-knowledge models for robotics,” *arXiv preprint arXiv:2401.12202*, 2024.
- [2] H. Xiong, R. Mendonca, K. Shaw, and D. Pathak, “Adaptive mobile manipulation for articulated objects in the open world,” *arXiv preprint arXiv:2401.14403*, 2024.
- [3] Z. Fu, T. Z. Zhao, and C. Finn, “Mobile aloha: Learning bimanual mobile manipulation with low-cost whole-body teleoperation,” *arXiv preprint arXiv:2401.02117*, 2024.
- [4] J. Wu, R. Antonova, A. Kan, M. Lepert, A. Zeng, S. Song, J. Bohg, S. Rusinkiewicz, and T. Funkhouser, “Tidybot: Personalized robot assistance with large language models,” *Autonomous Robots*, vol. 47, no. 8, pp. 1087–1102, 2023.
- [5] S. Bahl, A. Gupta, and D. Pathak, “Human-to-robot imitation in the wild,” *arXiv preprint arXiv:2207.09450*, 2022.
- [6] J.-P. Sleiman, F. Farshidian, and M. Hutter, “Versatile multicontact planning and control for legged loco-manipulation,” *Science Robotics*, vol. 8, no. 81, p. eadg5014, 2023.
- [7] N. Yokoyama, A. W. Clegg, E. Undersander, S. Ha, D. Batra, and A. Rai, “Adaptive skill coordination for robotic mobile manipulation,” *arXiv preprint arXiv:2304.00410*, 2023.
- [8] Z. Fu, X. Cheng, and D. Pathak, “Deep whole-body control: learning a unified policy for manipulation and locomotion,” in *Conference on Robot Learning*. PMLR, 2023, pp. 138–149.
- [9] J. Zhang, N. Gireesh, J. Wang, X. Fang, C. Xu, W. Chen, L. Dai, and H. Wang, “Gamma: Graspability-aware mobile manipulation policy learning based on online grasping pose fusion,” *arXiv preprint arXiv:2309.15459*, 2023.
- [10] R.-Z. Qiu, Y. Hu, G. Yang, Y. Song, Y. Fu, J. Ye, J. Mu, R. Yang, N. Atanasov, S. Scherer *et al.*, “Learning generalizable feature fields for mobile manipulation,” *arXiv preprint arXiv:2403.07563*, 2024.
- [11] G. B. Margolis, G. Yang, K. Paigwar, T. Chen, and P. Agrawal, “Rapid locomotion via reinforcement learning,” *arXiv preprint arXiv:2205.02824*, 2022.
- [12] R. Yang, Y. Kim, A. Kembhavi, X. Wang, and K. Ehsani, “Harmonic mobile manipulation,” *arXiv preprint arXiv:2312.06639*, 2023.
- [13] N. M. M. Shafiullah, C. Paxton, L. Pinto, S. Chintala, and A. Szlam, “Clip-fields: Weakly supervised semantic fields for robotic memory,” *arXiv preprint arXiv:2210.05663*, 2022.
- [14] J. Pari, N. M. Shafiullah, S. P. Arunachalam, and L. Pinto, “The surprising effectiveness of representation learning for visual imitation,” *arXiv preprint arXiv:2112.01511*, 2021.
- [15] Y. Ji, Z. Li, Y. Sun, X. B. Peng, S. Levine, G. Berseth, and K. Sreenath, “Hierarchical reinforcement learning for precise soccer shooting skills using a quadrupedal robot,” in *2022 IEEE/RSJ International Conference on Intelligent Robots and Systems (IROS)*. IEEE, 2022, pp. 1479–1486.
- [16] G. B. Margolis, X. Fu, Y. Ji, and P. Agrawal, “Learning to see physical properties with active sensing motor policies,” *arXiv preprint arXiv:2311.01405*, 2023.
- [17] J. Long, Z. Wang, Q. Li, L. Cao, J. Gao, and J. Pang, “The him solution for legged locomotion: Minimal sensors, efficient learning, and substantial agility,” in *The Twelfth International Conference on Learning Representations*, 2023.
- [18] R. Yang, Z. Chen, J. Ma, C. Zheng, Y. Chen, Q. Nguyen, and X. Wang, “Generalized animal imitator: Agile locomotion with versatile motion prior,” *arXiv preprint arXiv:2310.01408*, 2023.
- [19] G. B. Margolis, T. Chen, K. Paigwar, X. Fu, D. Kim, S. Kim, and P. Agrawal, “Learning to jump from pixels,” *arXiv preprint arXiv:2110.15344*, 2021.
- [20] A. Agarwal, A. Kumar, J. Malik, and D. Pathak, “Legged locomotion in challenging terrains using egocentric vision,” in *Conference on robot learning*. PMLR, 2023, pp. 403–415.
- [21] Z. Fu, A. Kumar, A. Agarwal, H. Qi, J. Malik, and D. Pathak, “Coupling vision and proprioception for navigation of legged robots,” in *Proceedings of the IEEE/CVF Conference on Computer Vision and Pattern Recognition*, 2022, pp. 17 273–17 283.
- [22] Z. Fu, A. Kumar, J. Malik, and D. Pathak, “Minimizing energy consumption leads to the emergence of gaits in legged robots,” *arXiv preprint arXiv:2111.01674*, 2021.
- [23] K. Lei, Z. He, C. Lu, K. Hu, Y. Gao, and H. Xu, “Uni-o4: Unifying online and offline deep reinforcement learning with multi-step on-policy optimization,” *arXiv preprint arXiv:2311.03351*, 2023.
- [24] R. Grandia, F. Jenelten, S. Yang, F. Farshidian, and M. Hutter, “Perceptive locomotion through nonlinear model-predictive control,” *IEEE Transactions on Robotics*, 2023.
- [25] N. Rathod, A. Bratta, M. Focchi, M. Zanon, O. Villarreal, C. Semini, and A. Bemporad, “Model predictive control with environment adaptation for legged locomotion,” *IEEE Access*, vol. 9, pp. 145 710–145 727, 2021.
- [26] V. Makoviychuk, L. Wawrzyniak, Y. Guo, M. Lu, K. Storey, M. Macklin, D. Hoeller, N. Rudin, A. Allshire, A. Handa *et al.*, “Isaac gym: High performance gpu-based physics simulation for robot learning,” *arXiv preprint arXiv:2108.10470*, 2021.
- [27] A. Kumar, Z. Fu, D. Pathak, and J. Malik, “Rma: Rapid motor adaptation for legged robots,” *arXiv preprint arXiv:2107.04034*, 2021.
- [28] R. Yang, M. Zhang, N. Hansen, H. Xu, and X. Wang, “Learning vision-guided quadrupedal locomotion end-to-end with cross-modal transformers,” *arXiv preprint arXiv:2107.03996*, 2021.
- [29] R. Yang, G. Yang, and X. Wang, “Neural volumetric memory for visual locomotion control,” in *Proceedings of the IEEE/CVF Conference on Computer Vision and Pattern Recognition*, 2023, pp. 1430–1440.
- [30] G. B. Margolis and P. Agrawal, “Walk these ways: Tuning robot control for generalization with multiplicity of behavior,” in *Conference on Robot Learning*. PMLR, 2023, pp. 22–31.
- [31] Z. Zhuang, Z. Fu, J. Wang, C. Atkeson, S. Schwertfeger, C. Finn, and H. Zhao, “Robot parkour learning,” *arXiv preprint arXiv:2309.05665*, 2023.
- [32] X. Cheng, K. Shi, A. Agarwal, and D. Pathak, “Extreme parkour with legged robots,” *arXiv preprint arXiv:2309.14341*, 2023.
- [33] J. Wang and E. Olson, “Apriltag 2: Efficient and robust fiducial detection,” in *2016 IEEE/RSJ International Conference on Intelligent Robots and Systems (IROS)*. IEEE, 2016, pp. 4193–4198.
- [34] E. Olson, “Apriltag: A robust and flexible visual fiducial system,” in *2011 IEEE international conference on robotics and automation*. IEEE, 2011, pp. 3400–3407.